centrifugation. Respiration and OXPHOS enzyme activities were normalized for protein concentration using the Coomassie Stain kit (Pierce)[13,19]. Mitochondrial membrane potential was calculated from mitochondrial uptake of TPP^+ using a TPP^+-sensitive electrode[12]. The sensitivity of the mtPTP to undergo permeability transition was examined in liver mitochondria of 10-month-old *Ant1*$^{-/-}$, *Ant2*$^{fl/Y}$, *Alb-Cre* animals by TPP^+ release after sequential additions of 10 nM $CaCl_2$ (ref. 13). The mtPTP modulators used were 1 mM *t*-H_2O_2, 0.1 mM diamide, 100 μM ATR and 125 μM ADP (Fig. 3).

Mitochondrial PTP activation was also monitored by mitochondrial swelling using light scattering at 546 nm for 10 min in 1.5 ml with 1 mg mitochondrial protein and 16.5 nmol $CaCl_2$. The reaction was initiated by the addition of 0.1 μM ruthenium red and 1 μM FCCP.

Hepatocytes were isolated from 12- to 15-month-old anaesthetized mice, perfused *in situ* with collagenase-dispase medium (Invitrogen). Hepatocytes were gently released, filtered and cultured on collagen-coated cover glasses or plates in Waymouth's MB-752/1 medium[17]. Hepatocyte sensitivity to Ca^{2+} ionophore was examined by extent of cell death assessed by the percentage of total cellular lactate dehydrogenase (LDH) released into the medium[20] after treatment with 5 to 50 μM Br-A23187 for 1 h, without or with a 30 min pretreatment of either 1 μM CsA or 50 μM z-VAD 17 (Fig. 4). Receptor-induced cell death was monitored by analysis of nuclear morphology using Hoechst 33258 (Molecular Probes) staining after treatment with 100 ng ml^{-1} of murine recombinant TNF-α (R&D Systems) or 4 ng ml^{-1} of human recombinant Fas ligand (Upstate), with or without 0.2 μg ml^{-1} actinomycin D (Fig. 4).

Received 14 August; accepted 10 November 2003; doi:10.1038/nature02229.

1. Zoratti, M. & Szabo, I. The mitochondrial permeability transition. *Biochim. Biophys. Acta* **1241,** 139–176 (1995).
2. Marzo, I. *et al.* Bax and adenine nucleotide translocator cooperate in the mitochondrial control of apoptosis. *Science* **281,** 2027–2031 (1998).
3. Levy, S. E., Chen, Y.-S., Graham, B. H. & Wallace, D. C. Expression and sequence analysis of the mouse adenine nucleotide translocase 1 and 2 genes. *Gene* **254,** 57–66 (2000).
4. Ellison, J. W., Salido, E. C. & Shapiro, L. J. Genetic mapping of the adenine nucleotide translocase-2 gene (*Ant2*) to the mouse proximal X chromosome. *Genomics* **36,** 369–371 (1996).
5. Graham, B. *et al.* A mouse model for mitochondrial myopathy and cardiomyopathy resulting from a deficiency in the heart/skeletal muscle isoform of the adenine nucleotide translocator. *Nature Genet.* **16,** 226–234 (1997).
6. Stepien, G., Torroni, A., Chung, A. B., Hodge, J. A. & Wallace, D. C. Differential expression of adenine nucleotide translocator isoforms in mammalian tissues and during muscle cell differentiation. *J. Biol. Chem.* **267,** 14592–14597 (1992).
7. Lunardi, J., Hurko, O., Engel, W. K. & Attardi, G. The multiple ADP/ATP translocase genes are differentially expressed during human muscle development. *J. Biol. Chem.* **267,** 15267–15270 (1992).
8. Postic, C. & Magnuson, M. A. DNA excision in liver by an albumin-Cre transgene occurs progressively with age. *Genesis* **26,** 149–150 (2000).
9. Boss, O., Hagen, T. & Lowell, B. B. Uncoupling proteins 2 and 3: potential regulators of mitochondrial energy metabolism. *Diabetes* **49,** 143–156 (2000).
10. Petronilli, V., Nicolli, A., Costantini, P., Colonna, R. & Bernardi, P. Regulation of the permeability transition pore, a voltage-dependent mitochondrial channel inhibited by cyclosporin A. *Biochim. Biophys. Acta* **1187,** 255–259 (1994).
11. Bernardi, P. Modulation of the mitochondrial cyclosporin A-sensitive permeability transition pore by the proton electrochemical gradient. Evidence that the pore can be opened by membrane depolarization. *J. Biol. Chem.* **267,** 8834–8839 (1992).
12. Esposito, L. A. *et al.* Mitochondrial oxidative stress in mice lacking the glutathione peroxidase-1 gene. *Free Radic. Biol. Med.* **28,** 754–766 (2000).
13. Kokoszka, J. E., Coskun, P., Esposito, L. & Wallace, D. C. Increased mitochondrial oxidative stress in the $Sod2^{+/-}$ mouse results in the age-related decline of mitochondrial function culminating in increased apoptosis. *Proc. Natl Acad. Sci. USA* **98,** 2278–2283 (2001).
14. Halestrap, A. P., Woodfield, K. Y. & Connern, C. P. Oxidative stress, thiol reagents, and membrane potential modulate the mitochondrial permeability transition by affecting nucleotide binding to the adenine nucleotide translocase. *J. Biol. Chem.* **272,** 3346–3354 (1997).
15. Lapidus, R. G. & Sokolove, P. M. The mitochondrial permeability transition. Interactions of spermine, ADP, and inorganic phosphate. *J. Biol. Chem.* **269,** 18931–18936 (1994).
16. Novgorodov, S. A., Gudz, T. I., Brierley, G. P. & Pfeiffer, D. R. Magnesium ion modulates the sensitivity of the mitochondrial permeability transition pore to cyclosporin A and ADP. *Arch. Biochem. Biophys.* **311,** 219–228 (1994).
17. Qian, T., Herman, B. & Lemasters, J. J. The mitochondrial permeability transition mediates both necrotic and apoptotic death of hepatocytes exposed to Br-A23187. *Toxicol. Appl. Pharmacol.* **154,** 117–125 (1999).
18. Hatano, E. *et al.* The mitochondrial permeability transition augments Fas-induced apoptosis in mouse hepatocytes. *J. Biol. Chem.* **275,** 11814–11823 (2000).
19. Trounce, I. A., Kim, Y. L., Jun, A. S. & Wallace, D. C. Assessment of mitochondrial oxidative phosphorylation in patient muscle biopsies, lymphoblasts, and transmitochondrial cell lines. *Methods Enzymol.* **264,** 484–509 (1996).
20. Leist, M. *et al.* Murine hepatocyte apoptosis induced *in vitro* and *in vivo* by TNF-α requires transcriptional arrest. *J. Immunol.* **153,** 1778–1788 (1994).

Acknowledgements We thank M. Magnuson for providing the *Alb-Cre* transgenic mice, L. Hayes for mouse husbandry and genotyping, and H. Yi for the electron microscope analysis. This work was funded by US National Institutes of Health grants awarded to D.C.W., G.R.M. and D.P.J.

Competing interests statement The authors declare competing financial interests: details accompany the paper on **www.nature.com/nature**.

Correspondence and requests for materials should be addressed to D.C.W. (dwallace@uci.edu).

Mechanically driven ATP synthesis by F_1-ATPase

Hiroyasu Itoh[1,2], Akira Takahashi[3], Kengo Adachi[4], Hiroyuki Noji[5], Ryohei Yasuda[6], Masasuke Yoshida[7] & Kazuhiko Kinosita Jr[4]

[1]*Tsukuba Research Laboratory, Hamamatsu Photonics KK, and* [2]*CREST "Creation and application of soft nano-machine, the hyperfunctional molecular machine" Team 13*, Tokodai, Tsukuba 300-2635, Japan*
[3]*System Division, Hamamatsu Photonics KK, Joko, Hamamatsu 431-3103, Japan*
[4]*Center for Integrative Bioscience, Okazaki National Research Institutes, Okazaki 444-8585, Japan*
[5]*Institute of Industrial Science, University of Tokyo, Tokyo 153-8505, Japan*
[6]*Cold Spring Harbor Laboratory, Cold Spring Harbor, New York 11724 USA*
[7]*ERATO "ATP System", 5800-3 Nagatsuta, Yokohama 226-0026, Japan*

ATP, the main biological energy currency, is synthesized from ADP and inorganic phosphate by ATP synthase in an energy-requiring reaction[1–3]. The F_1 portion of ATP synthase, also known as F_1-ATPase, functions as a rotary molecular motor: *in vitro* its γ-subunit rotates[4] against the surrounding $\alpha_3\beta_3$ subunits[5], hydrolysing ATP in three separate catalytic sites on the β-subunits. It is widely believed that reverse rotation of the γ-subunit, driven by proton flow through the associated F_o portion of ATP synthase, leads to ATP synthesis in biological systems[1–3,6,7]. Here we present direct evidence for the chemical synthesis of ATP driven by mechanical energy. We attached a magnetic bead to the γ-subunit of isolated F_1 on a glass surface, and rotated the bead using electrical magnets. Rotation in the appropriate direction resulted in the appearance of ATP in the medium as detected by the luciferase–luciferin reaction. This shows that a vectorial force (torque) working at one particular point on a protein machine can influence a chemical reaction occurring in physically remote catalytic sites, driving the reaction far from equilibrium.

When isolated F_1 hydrolyses ATP, its central γ-subunit rotates anticlockwise[4] when viewed from above in Fig. 1a, with an efficiency of chemical-to-mechanical energy conversion approaching 100% (ref. 8). The purpose of this study was to show that the chemo-mechanical coupling in the F_1 motor is completely reversible, and that reversal is achieved by manipulating a single variable—that is, the rotary angle of the γ-subunit. Any molecular machine would be reversible if one could manipulate all constituent atoms at will. Whether one or a few thermodynamic handles exist in a chemo-mechanical molecular machine such that its operation can be controlled through that handle in both directions is an important but unresolved issue. For example, whether one can synthesize ATP by pulling back a linear molecular motor such as myosin or kinesin—and if so, where to pull—is unknown. Reversal of the whole ATP synthase is well documented[1,9], including the demonstration of γ-subunit reorientation under synthesis conditions[10], but whether or not the γ-subunit angle serves as a single handle for F_1 reversal has not been tested.

To prove this reversibility, we used $\alpha_3\beta_3\gamma$, the minimal subcomplex of F_1 that shows ATP-catalysed rotation[4]. The subcomplex was attached to a glass surface through histidine residues engineered at the amino terminus of the β-subunits, and a magnetic bead coated with streptavidin was attached to the γ-subunit, which had been biotinylated at two engineered cysteines (Fig. 1a). The beads were rotated with magnets (Fig. 1b–d) in a medium containing ADP and phosphate as substrates and the luciferin–luciferase system[11,12], which emits a photon when it captures and hydrolyses ATP. The initial idea was to count these chemiluminescent photons (Fig. 1b); however, background luminescence originating from contaminant ATP present in ADP even after purification was a problem. Thus, the

volume of medium per active F_1 molecule had to be small.

First, we tried to reduce the volume by making microdroplets in oil (Fig. 2a). Figure 2b shows data from a 4×4 array of droplets in one chamber. The beads in droplets were rotated at 10 Hz alternately for 5 min each in the direction of hydrolysis (anticlockwise when viewed from top in Fig. 1a) and synthesis (clockwise). As seen in Fig. 2b, 14 out of 16 droplet curves showed the M-shaped pattern of photon counts expected for the sequence of rotation direction when the overall decline was taken into account. The decline was due to the gradual disappearance of the aqueous phase into oil: although we saturated the oil with water before the experiment, droplets tended to shrink over time. For random photon counts, the probability of observing a slanting M shape is 8^{-1}. The probability of observing 14 or more M shapes out of 16 is 2×10^{-11}. The data set shown in Fig. 2b thus strongly indicates mechanical synthesis. The experiment is extremely difficult (at most a few beads rotate in each droplet), however, and we have obtained only a few more data sets that contained several M-shaped patterns.

We thus tried to increase the number of rotating beads in an ordinary observation chamber (Fig. 1c) by infusing a concentrated solution of beads carrying F_1. To allow F_1 to rotate in the proper direction, we derivatized only the bottom surface of the chamber with nickel nitrilo-triacetic acid (Ni^{2+}-NTA), which would specifically bind the β-histidines. In control experiments done in 4 mM ATP (no ADP) and without magnets, we found in the field of view of $1.0 \times 10^5\ \mu m^2$ as many as 480 ± 70 F_1 molecules rotating anticlockwise at the bottom (three chambers). However, the high density of beads resulted in nonspecific binding to the ceiling, where 100 ± 20 beads rotated clockwise (as viewed from above the chamber). We also tested in the ATP medium whether forced rotation by external magnets would damage F_1. After confirming ATP-driven rotation, we turned on the magnets and applied several bursts of hundreds of revolutions at 10 Hz in both directions. When the magnets were turned off, ATP-driven rotation resumed.

Synthesis was shown in the ADP–luciferase medium by accumulating chemiluminescence photons over a series of 5-min intervals in which the magnetic field was rotated at 10 Hz in either direction or turned off. All series produced the expected pattern (Fig. 3a): higher photon counts during clockwise rotation (S, synthesis) than during anticlockwise rotation (H, hydrolysis) or no rotation (N). This graph compiles all data taken in consecutive experiments (about half of the experiments failed at some point, for example during chamber preparation or because of a large focus drift, and did not produce data). Mechanical synthesis in the flat chamber was reproducible, although variation among data was still large.

We note that in most curves shown in Fig. 3a including the total counts, counts during anticlockwise rotation (H) are higher than those at no rotation (N). This is due to the presence of F_1 at the ceiling of the chamber as stated above. For these upside-down F_1 molecules, anticlockwise bead rotation will drive ATP synthesis. Indeed, when we flipped the chamber upside down after obtaining the unbroken blue line in Fig. 3a, the count pattern was reversed, as shown by the broken blue line. Another reason for the higher counts during anticlockwise rotation was that luciferase did not consume all of the newly synthesized ATP in 5 min: as shown by the unbroken lines in Fig. 3b, the luminescence at no rotation was high after ATP synthesis at the arrows. Luminescence decay after ATP mixing was shown to involve a component with a lifetime of about 3 min (see Supplementary Information). Taking all of the above points into account, we consider that mechanical synthesis has been conclusively demonstrated.

Figure 4 shows the effect of rotary speed on the efficiency of ATP synthesis. The synthesis rate apparently saturated above 3 Hz (Fig. 4b). This was because larger beads or bead aggregates failed to rotate at high speeds, as confirmed by direct observation (uncoupling between magnet and bead rotations). Calibration of the

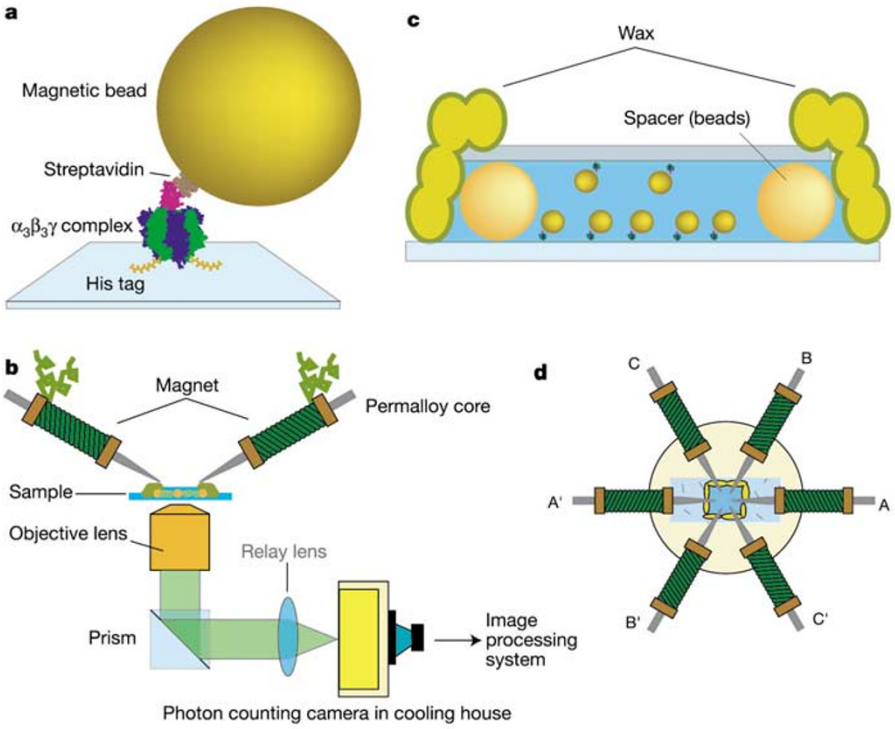

Figure 1 Experimental set-up. **a**, Basic design. The structures of F_1 and streptavidin are from ref. 21 and ref. 22, respectively. The bead is not to scale and the orientation of streptavidin is unknown. **b**, Side view of the optical system. **c**, Observation chamber. Ni^{2+}-NTA was applied only to the bottom surface, but some F_1-conjugated beads rotated on the ceiling. **d**, Top view of the magnets.

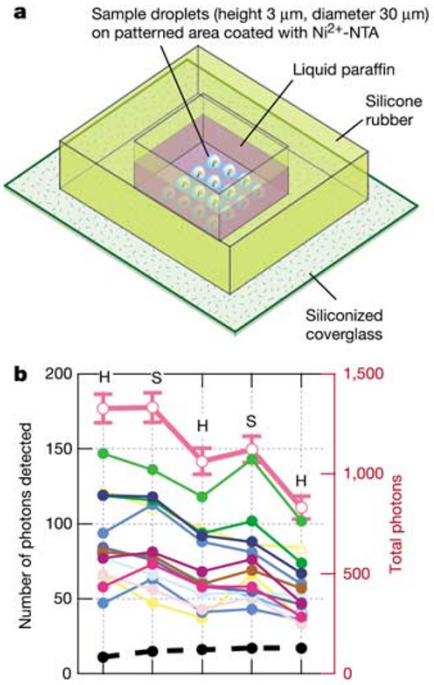

Figure 2 Rotational synthesis in microdroplets. **a**, Observation chamber. On the silanized bottom coverglass, 4 × 4 spots separated by ~50 μm and measuring 20–30 μm were derivatized with Ni^{2+}-NTA, which rendered the spots hydrophilic. An oil layer with a thickness of ~3 mm was placed on top. Using a glass micropipette, we formed a droplet of ~1 pl containing F_1 on each spot and then replaced the solution with one containing beads, ADP, phosphate and the chemiluminescence system. **b**, Simultaneous observation of 16 droplets. Thick magenta curve with open circles represents the sum of all unbroken curves; error bars represent ± 2σ, where σ is the expected s.d. for photon statistics (square root of the total count). The broken curve at the bottom represents a control in which an area outside the droplets was imaged. See Supplementary Information for details.

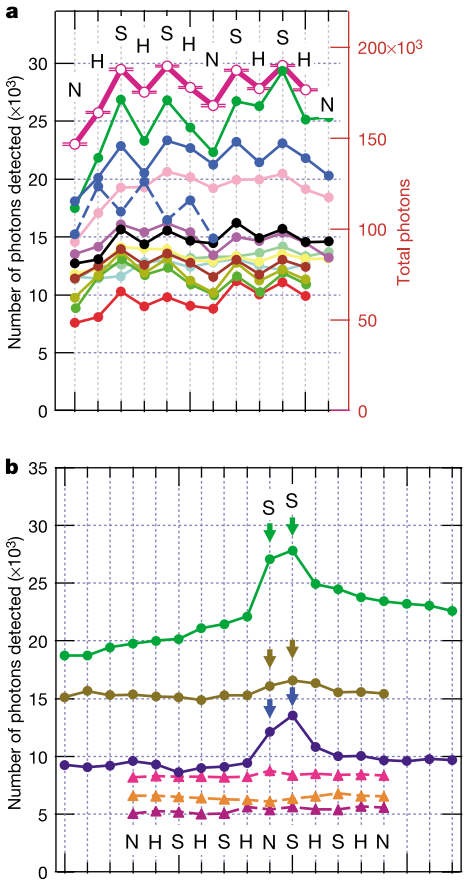

Figure 3 Rotational synthesis in a flat chamber. Each symbol shows the number of photons detected over 5 min in an image area of 7.8 × 10^4 μm^2. N, no rotation; H, 10-Hz rotation in the hydrolysis direction (for F_1 on the bottom of the chamber); S, 10-Hz rotation in the synthesis direction. **a**, Results from 12 chambers, distinguished by different colours. Broken blue curve represents results obtained after the chamber giving rise to the unbroken blue curve was flipped upside down. Thick magenta curve with open circles represents the sum of all unbroken curves; error bars represent ± 4σ (>99.99% confidence). For clarity, some curves have been shifted vertically within ± 1,000 counts. **b**, Control experiments. Unbroken curves show results either without rotation or with imposed clockwise rotation for synthesis at 10 Hz (arrows). Broken curves show experiments carried out as in **a** except that phosphate was omitted from the medium. The counts in the broken curves are low in comparison to the others because phosphate tended to increase the background, apparently by increasing the portion of luciferase that reacted with ATP extremely slowly (see Supplementary Information).

photon-to-ATP ratio (see Supplementary Information) indicated a synthesis rate of about five molecules of ATP per second under rotation at 3 Hz, as compared with the nine molecules of ATP per second expected for the one ATP molecule per 120° scheme[8].

Although Fig. 4 represents our best data so far and variation among chambers is large (Fig. 3a), we anticipate that the coupling between mechanical rotation of the γ-subunit and chemical synthesis is tight, at least at low speeds. The significant synthesis at low speeds (Fig. 4), which were much lower than the maximal rotary speed of 130 Hz of this motor during ATP hydrolysis[13], merits attention. Because the slow rotation was at a constant speed, it is likely that chemical reactions were at quasi-equilibrium at all angles. Rotation by ATP hydrolysis can also be made slow and at a constant speed by attaching a long actin filament to the γ-subunit[8], again suggesting quasi-equilibrium. The implication is that ATP synthesis in F_1 proceeds as a straightforward reversal of the hydrolysis reaction, tracking the same reaction pathway in the opposite direction. On that pathway, both hydrolysis and synthesis reactions are controlled by one mechanical handle, the rotary angle of the γ-subunit. The situation contrasts with the more complex rotary motor of bacterial flagella, where rotational directions can be switched without reversing the proton motive force[14].

ATP synthesis is a chemical reaction that is energetically uphill, requiring 80–100 pN nm of energy under physiological conditions[2]. In the experiments shown here, contaminant ATP amounted to about 1 nM, implying that roughly 30 pN nm of free energy was needed per molecule of ATP synthesized (see Supplementary Information). If F_1, or the motor enzyme myosin, is mixed with high concentrations of ADP and phosphate in the absence of ATP, some ATP is spontaneously formed on the enzyme without input of energy[15–18]. This, however, is a dead-end reaction and the ATP that has been formed is not available in the medium: release of the tightly bound ATP requires an external supply of energy[1,13].

Here we have demonstrated repetitive synthesis by F_1 (~10^3 ATP molecules in 5 min), leading to appearance of the product in the medium. To our knowledge, this is the first accomplishment of artificial chemical synthesis by a vectorial force (although nature presumably has been doing this for millions of years). Pressure could also shift a chemical equilibrium by acting on substrates (and solvent); however, in our experiments the chemical equilibrium *per se* is on the side of almost complete hydrolysis, and a force on a point remote from substrates counters the hydrolysis reaction and pushes the equilibrium to the point of favouring synthesis. Because we still have to rely on nature's nanomachine, the F_1 motor, our

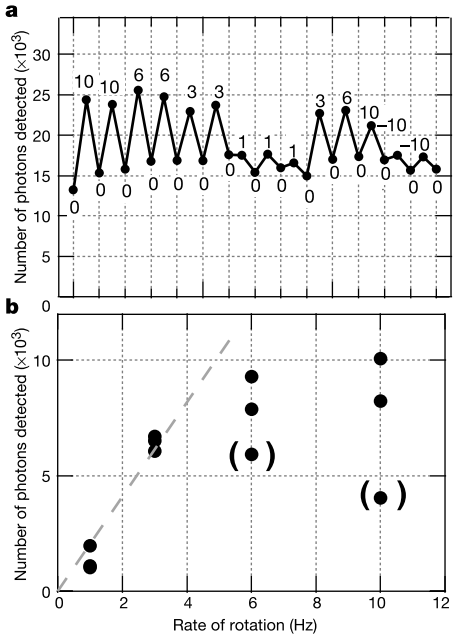

Figure 4 Dependence of synthesis efficiency on the rate of magnet rotation. **a**, Photons detected over an image area of 1.0×10^5 μm^2 in 5-min periods at various rotary speeds (shown in Hz; negative numbers indicate rotation in the hydrolysis direction). **b**, Photon increments during rotation. From the photon count for each synthesis rotation in **a**, the average of the adjacent no-rotation counts was subtracted. Symbols in the parentheses show the last two measurements for synthesis in **a**; low values for these presumably reflect sample deterioration.

primary goal is to understand fully how it works and thereby to exploit the mechanism in artificial ways. Improving the present system for more quantitative assays, such as the torque and speed dependence of the coupling efficiency, that can be compared with theoretical predictions[7,19] should be our next task. The key is to obtain magnetic beads that are small and uniform in size. □

Methods

Materials

A mutant $\alpha_3\beta_3\gamma$ subcomplex (comprising C193S α-, His_{10}–β-, and S107C, I210C γ-subunits; referred to as F_1 in this paper), derived from the thermophilic *Bacillus* strain PS3, was biotinylated at the only cysteines on the γ-subunit (ref. 8). Streptavidin-coated magnetic beads (Seradyn; nominally 0.7 μm) were lightly centrifuged to remove large beads and aggregates (but elimination was incomplete). Biotinylated F_1 (400 pM) was incubated with beads (~50 pM) in buffer A (50 mM 3-(*N*-morpholino)propanesulphonic acid/KOH, 20 mM K_2SO_4, 4 mM $MgSO_4$, pH 7.6) for 10 min at 23 °C, washed with buffer A, and concentrated with a magnet. Luciferase[12] was a kind gift from Kikkoman Co. We purified ADP (K-salt; Sigma) as described[20] on a Poros HQ/L column (Applied Biosystems).

Observation chamber

For the chamber shown in Fig. 1c, a 32×24 mm^2 coverglass was functionalized by a silane coupling agent with an SH group (TSL 8380; GE Toshiba Silicone), and reacted first with 10 mg ml^{-1} maleimide-C_3-NTA (Dojindo) and then with 10 mM $NiCl_2$. Two parallel strips of Lumirror polyester film (TORAY) were placed on the coverglass, and a 18×18 mm^2 coverglass coated with hexamethyldisilazane was placed on top to form a flow chamber. We infused ~500 pM F_1-conjugated magnetic beads in buffer A_3 (buffer A containing 3 mg ml^{-1} bovine serum albumin (BSA)) and incubated the chamber for 30 min at 23 °C. After infusing buffer A_3 several times, buffer A containing 10 μM luciferase, 1 mM luciferin, 10 mM K_2PO_4, 200 μM ADP and 1.5 mg ml^{-1} BSA, together with a small number of 3-μm Dynabeads M-280 beads (Dynal) that would eventually serve as spacers, was infused. The spacer strips were carefully removed and the upper coverglass was pressed to reduce the chamber height to ~3 μm, as determined by the spacer beads. The chamber was then sealed with wax and subjected to observation.

Microscopy

The chamber was placed on an inverted ICM 450 microscope (Zeiss). Luminescence was collected with an oil immersion ×60 objective, numerical aperture 1.45 (Olympus) and deflected with a prism to a factory-made side port (Fig. 1b). The beam was focused with an ED Plan ×2 objective (Nikon) onto a cooled photon-counting camera (V8070U-64-N230/C4566 equipped with an Argus 50 image processing system; Hamamatsu Photonics), which recorded centroid positions of incoming photons (counts in the dark: ~15 s^{-1} over the whole image plane). To rotate the beads, we placed three opposing pairs of custom-made electromagnets with a Permalloy core on the chamber (Fig. 1d). The three pairs were activated with a custom circuit 120° out of phase to produce a rotating magnetic field (in either direction).

Received 5 May; accepted 31 October 2003; doi:10.1038/nature02212.

1. Boyer, P. D. The ATP synthase—a splendid molecular machine. *Annu. Rev. Biochem.* **66,** 717–749 (1997).
2. Kinosita, K. Jr, Yasuda, R., Noji, H. & Adachi, K. A rotary molecular motor that can work at near 100% efficiency. *Phil. Trans. R. Soc. Lond. B* **355,** 473–489 (2000).
3. Yoshida, M., Muneyuki, E. & Hisabori, T. ATP synthase—a marvellous rotary engine of the cell. *Nature Rev. Mol. Cell Biol.* **2,** 669–677 (2001).
4. Noji, H., Yasuda, R., Yoshida, M. & Kinosita, K. Jr Direct observation of the rotation of F_1-ATPase. *Nature* **386,** 299–302 (1997).
5. Abrahams, J. P., Leslie, A. G. W., Lutter, R. & Walker, J. E. Structure at 2.8 Å resolution of F_1-ATPase from bovine heart mitochondria. *Nature* **370,** 621–628 (1994).
6. Boyer, P. D. & Kohlbrenner, W. E. in *Energy Coupling in Photosynthesis* (eds Selman, B. R. & Selman-Reimer, S.) 231–240 (Elsevier, Amsterdam, 1981).
7. Oosawa, F. & Hayashi, S. The loose coupling mechanism in molecular machines of living cells. *Adv. Biophys.* **22,** 151–183 (1986).
8. Yasuda, R., Noji, H., Kinosita, K. Jr & Yoshida, M. F_1-ATPase is a highly efficient molecular motor that rotates with discrete 120° steps. *Cell* **93,** 1117–1124 (1998).
9. Turina, P., Samoray, D. & Gräber, P. H^+/ATP ratio of proton transport-coupled ATP synthesis and hydrolysis catalysed by CF_0F_1-liposomes. *EMBO J.* **22,** 418–426 (2003).
10. Zhou, Y., Duncan, T. M. & Cross, R. L. Subunit rotation in *Escherichia coli* F_oF_1–ATP synthase during oxidative phosphorylation. *Proc. Natl Acad. Sci. USA* **94,** 10583–10587 (1997).
11. McElroy, W. D., Seliger, H. H. & White, E. H. Mechanism of bioluminescence, chemiluminescence and enzyme function in the oxidation of firefly luciferin. *Photochem. Photobiol.* **10,** 153–170 (1969).
12. Hattori, N., Kajiyama, N., Maeda, M. & Murakami, S. Mutant luciferase enzymes from fireflies with increased resistance to benzalkonium chloride. *Biosci. Biotechnol. Biochem.* **66,** 2587–2593 (2002).
13. Yasuda, R., Noji, H., Yoshida, M., Kinosita, K. Jr & Itoh, H. Resolution of distinct rotational substeps by submillisecond kinetic analysis of F_1-ATPase. *Nature* **410,** 898–904 (2001).
14. Berg, H. C. The rotary motor of bacterial flagella. *Annu. Rev. Biochem.* **72,** 19–54 (2003).
15. Yoshida, M. The synthesis of enzyme-bound ATP by the F_1-ATPase from the thermophilic bacterium PS3 in 50% dimethylsulfoxide. *Biochem. Biophys. Res. Commun.* **114,** 907–912 (1983).
16. Sakamoto, J. Effect of dimethylsulfoxide on ATP synthesis by mitochondrial soluble F_1-ATPase. *J. Biochem.* **96,** 483–487 (1984).
17. Wolcott, R. G. & Boyer, P. D. The reversal of the myosin and actomyosin ATPase reactions and the free energy of ATP binding to myosin. *Biochem. Biophys. Res. Commun.* **57,** 709–716 (1974).
18. Mannherz, H. G., Schenck, H. & Goody, R. S. Synthesis of ATP from ADP and inorganic phosphate at the myosin-subfragment 1 active site. *Eur. J. Biochem.* **48,** 287–295 (1974).
19. Wang, H. & Oster, G. Energy transduction in the F_1 motor of ATP synthase. *Nature* **396,** 279–282 (1998).
20. Oishi, N. & Sugi, H. *In vitro* ATP-dependent F-actin sliding on myosin is not infuenced by substitution or removal of bound nucleotide. *Biochim. Biophys. Acta* **1185,** 346–349 (1994).
21. Menz, R. I., Walker, J. E. & Leslie, A. G. W. Structure of bovine mitochondrial F_1-ATPase with nucleotide bound to all three catalytic sites: implications for the mechanism of rotary catalysis. *Cell* **106,** 331–341 (2001).
22. Freitag, S., Trong, I. L., Klumb, L., Stayton, P. S. & Stenkamp, R. E. Structural studies of the streptavidin binding loop. *Protein Sci.* **6,** 1157–1166 (1997).

Supplementary Information accompanies the paper on **www.nature.com/nature**.

Acknowledgements We thank T. Hayakawa and T. Hiruma of Hamamatsu Photonics KK who allowed H.I. to work on this project for more than 6 years; S. Brenner for the idea of using microdroplets; M. Sugai for initial work; M. Shio, members of the former CREST Team 13 and the current Kinosita and Yoshida laboratories for help and advice; I. Mizuno, K. Suzuki, S. Uchiyama and Y. Mizuguchi for the photon-counting system; C. Gosse and H. Miyajima for the magnetic tweezers; K. Abe and K. Rikukawa for microscopy; S. Murakami for luciferase; and H. Umezawa and M. Fukatsu for laboratory management. This work was supported in part by Grants-in-Aid from the Ministry of Education, Culture, Sports, Science and Technology of Japan, and Burroughs Wellcome Fund (R.Y.).

Competing interests statement The authors declare that they have no competing financial interests.

Correspondence and requests for materials should be addressed to H.I. (hiritoh@hpk.trc-net.co.jp).